Acta Biomaterialia 142 (2022) 36–48

Contents lists available at ScienceDirect

Acta Biomaterialia

journal homepage: www.elsevier.com/locate/actbio

Full length article

Interpenetrating gallol functionalized tissue adhesive hyaluronic acid hydrogel polarizes macrophages to an immunosuppressive phenotype

Sumanta Samanta[a,1], Vignesh K. Rangasami[a,b,1], Heela Sarlus[c], Jay R.K. Samal[a,d], Austin D. Evans[a], Vijay S. Parihar[a], Oommen P. Varghese[b], Robert A. Harris[c], Oommen P. Oommen[a,*]

[a] Bioengineering and Nanomedicine Group, Faculty of Medicine and Health Technologies, Tampere University and BioMediTech Institute, 33720, Tampere, Finland
[b] Translational Chemical Biology Laboratory, Department of Chemistry, Ångström Laboratory, Uppsala University, 751 21, Uppsala, Sweden
[c] Applied Immunology and Immunotherapy, Department of Clinical Neuroscience, Karolinska Institutet, Stockholm, Centre for Molecular Medicine, Karolinska University Hospital, 171 76, Solna, Stockholm, Sweden
[d] Department of Instructive Biomaterial Engineering, MERLN Institute for Technology-Inspired Regenerative Medicine, Maastricht University, Maastricht, 6229 ER, Netherlands

ARTICLE INFO

Article history:
Received 11 November 2021
Revised 19 January 2022
Accepted 20 January 2022
Available online 24 January 2022

Keywords:
Hyaluronic acid
Gallic acid
Tissue-adhesive hydrogel
Interpenetrating network
Macrophage polarization

ABSTRACT

Innovative scaffold designs that modulate the local inflammatory microenvironment through favorable macrophage polarization and suppressing oxidative stress are needed for successful clinical translation of regenerative cell therapies and graft integration. We herein report derivation of a hydrazone-crosslinked gallol functionalized hyaluronic acid (HA-GA)-based hydrogel that displayed outstanding viscoelastic properties and immunomodulatory characteristics. Grafting of 6% gallol (GA) to a HA-backbone formed an interpenetrative network by promoting an additional crosslink between the gallol groups in addition to hydrazone crosslinking. This significantly enhanced the mechanical stability and displayed shear-thinning/self-healing characteristics, facilitated tissue adhesive properties to porcine tissue and also displayed radical scavenging properties, protecting encapsulated fibroblasts from peroxide challenge. The THP-1 human macrophage cell line or primary bone-marrow-derived murine macrophages cultured within HA-GA gels displayed selective polarization to a predominantly anti-inflammatory phenotype by upregulating IL4ra, IL-10, TGF-β, and TGF-βR1 expression when compared with HA-HA gels. Conversely, culturing of pro-inflammatory activated primary murine macrophages in HA-GA gels resulted in a significant reduction of pro-inflammatory TNF-α, IL-1β, SOCS3 and IL-6 marker expression, and upregulated expression of anti-inflammatory cytokines including TGF-β. Finally, when the gels were implanted subcutaneously into healthy mice, we observed infiltration of pro-inflammatory myeloid cells in HA-HA gels, while immunosuppressive phenotypes were observed within the HA-GA gels. Taken together these data suggest that HA-GA gels are an ideal injectable scaffold for viable immunotherapeutic interventions.

Statement of significance

Host immune response against the implanted scaffolds that are designed to deliver stem cells or therapeutic proteins in vivo significantly limits the functional outcome. For this reason, we have designed immunomodulatory injectable scaffolds that can favorably polarize the recruited macrophages and impart antioxidant properties to suppress oxidative stress. Specifically, we have tailored a hyaluronic acid-based extracellular matrix mimetic injectable scaffold that is grafted with immunomodulatory gallol moiety. Gallol functionalization of hydrogel not only enhanced the mechanical properties of the scaffold by form-

* Corresponding author.
E-mail addresses: oommen.oommen@tuni.fi (O.P. Varghese), oommen.oommen@tuni.fi (O.P. Oommen).
[1] Authors contributed equally.

https://doi.org/10.1016/j.actbio.2022.01.048
1742-7061/© 2022 The Author(s). Published by Elsevier Ltd on behalf of Acta Materialia Inc. This is an open access article under the CC BY license (http://creativecommons.org/licenses/by/4.0/)

ing an interpenetrating network but also induced antioxidant properties, tissue adhesive properties, and polarized primary murine macrophages to immunosuppressive phenotype. We believe such immunoresponsive implants will pave the way for developing the next-generation of biomaterials for regenerative medicine applications.

© 2022 The Author(s). Published by Elsevier Ltd on behalf of Acta Materialia Inc.
This is an open access article under the CC BY license (http://creativecommons.org/licenses/by/4.0/)

1. Introduction

During recent years there has been an exponential increase in the biomaterial research field of developing extracellular matrix-derived biopolymers for engineering bioactive scaffolds [1,2], nanocarriers [3] and other biomedical implants [4]. Several biomaterials trigger a cascade of cellular events that are initiated post-implantation by fibrinogen deposition, followed by neutrophil infiltration and monocyte recruitment that differentiate into macrophages in the tissue and cause inflammation and scar tissue formation [5]. The inflammation caused by these cellular and molecular events at the implant site is identified as a key bottleneck for using biomaterials for tissue engineering or as medical implants [6]. Excessive inflammation triggered by the host immune system can cause tissue destruction or poor implant integration, leading to failure or rejection. Similarly, the survival of encapsulated cells in these biomaterials poses a great challenge as the encapsulated cells undergo oxidative stress during inflammatory reactions, leading to poor cell survival and function [7,8]. There is thus a pressing need to engineer scaffolds with inherent antioxidant properties that will not only suppress oxidative stress but also suppress senescence and improve self-renewal [8].

Cells of the innate immune system such as macrophages are believed to be early responders in an immune response that dictates the success of implant integration [9]. Macrophages exist as specialized guardians in our tissues (tissue-resident cells) or are differentiated from circulating blood monocytes following immune activati [10]. They act as phagocytes as well as antigen-presenting cells, activating the adaptive immune system. Macrophages have been traditionally considered to be polarized into differential functional states that either broadly lead to tissue damage (pro-inflammatory or M1 macrophages) or immune suppression and tissue-healing macrophages (immunosuppressive or M2 macrophages) [11], although these properties are disease context-specific and the modern view reflects a spectrum of activation states.

Controlling or regulating the immune response by tuning macrophage activation at the implant site is one of the key challenges in biomaterials research [12]. Macrophages have enormous plasticity and their activation states can be modulated in response to the biophysical and biochemical cues encompassed in the injured or inflamed tissue [13,14]. The most common strategy to control this activation is by encapsulating specific signaling molecules or stimulants that dictate the phenotype of infiltrating monocytes following implantation [12]. For example, a pro-inflammatory macrophage activation state can be induced by IFN-γ, TNF-α, or endotoxin lipopolysaccharide (LPS), while an immunosuppressive macrophage activation state can be induced by IL-4, IL-10, IL-13 or by using a cocktail of cytokines such as M-CSF, IL-4, IL-10, and TGF-β [15,16].

Although these immunoregulatory strategies could be very useful for regulating the fate of the infiltrating cells, the cytokines used for developing the immune responsive scaffolds have limited half-life and are also expensive. Most of the 3D scaffolds derived from biopolymers such as chitosan [17] or alginate [18] themselves induce pro-inflammatory activation of macrophages. Conversely, scaffolds that selectively increase the population of immunosuppressive macrophages significantly improve the compatibility of the material for in vivo applications [19]. However, there is currently a paucity of scaffolds with the latter function.

In this report we address this challenge by engineering tissue instructive scaffolds utilizing extracellular matrix (ECM) polymers possessing appropriate physicochemical properties that modulate the host inflammatory response and ameliorate adverse immune reactions [20]. Hyaluronic acid (HA) is one such biopolymer and an important component of the ECM that is known to possess immune-responsive properties and could be used to fabricate bioactive nanomaterials and hydrogels.

From an engineering perspective, HA offers great advantages as it possesses several reactive functional groups that allow the conjugation of biorthogonal moieties and bioactive molecules. HA of different molecular weights have been reported to differentially activate macrophages [21] and HA-derived nanoparticles loaded with doxorubicin have been designed to regulate macrophage polarization [22]. HA-based nanoparticles have also been developed to target pro-inflammatory macrophages by targeting CD44 receptors [23] and are proposed for atherosclerosis treatment [24].

We have previously designed several drug delivery systems [25,26] and hydrogels [27,28] using HA as the base material. We have recently demonstrated that HA could effectively complex with nucleic acids through hydrophobic interactions [29], and that scaffolds tailored using HA possess growth factor-sequestering properties [30]. These scaffolds inherently do not change the immune-activating behavior of the materials and therefore have their limitations.

Herein, we aimed to overcome this problem by designing an HA-based scaffold with optimal biochemical cues that could differentiate infiltrating monocytes into immunosuppressive macrophages, achieved without the necessity of loading any immunoregulatory molecules. We believe such immunosuppressive scaffolds will be better tolerated for tissue regeneration applications.

2. Materials and methods

Hyaluronic acid (MW 130 kDa) was purchased from LifeCore Biomedical (Chaska, USA). Gallic acid (3,4,5-trihydroxy benzoic acid), 1-ethyl-3-(3-dimethyl aminopropyl)-carbodiimide hydrochloride (EDC), 1–hydroxy benzotriazole hydrate (HOBt), carbohydrazide (CDH), 3- amino 1,2- propanediol, and sodium periodate were purchased from Sigma-Aldrich. Dialysis membranes used for purification were purchased from Spectra Por-6 (MWCO 3500). All solvents were of analytical quality. All spectrophotometric analysis was carried out on Shimadzu UV-3600 plus UV–VIS-NIR spectrophotometer.

2.1. Hydrogel preparation

HA-HA and HA-GA hydrogels were prepared using hydrazone crosslinking between aldehyde and carbodihydrazide moieties of the hyaluronic acid derivative. The details of the synthesis and characterizations of the hyaluronic acid components, HA-CDH, HA-Ald, and HA-GA-CDH are described in the supporting information.

The components were dissolved at a concentration of 16 mg/mL for all experiments, and equal volumes of aldehyde and carbodihydrazide derivatives were used to form the hydrogels. HA-CDH and HA-GA-CDH were dissolved in 10% sucrose solution, while HA-Ald was dissolved in phosphate-buffered saline (1x PBS). Prior to experiments involving cell encapsulation, the materials were UV sterilized for 20 min and subsequently dissolved in sterile solutions.

2.2 Rheological properties

Hydrogels of 250 µL volume were prepared in the form of cylinders with 12 mm diameter, cured overnight and their rheological property was measured using a TA instruments' TRIOS Discovery HR 2 rheometer. The values for storage and loss modulus were obtained using the frequency sweep and were plotted against the frequency (Hz). This demonstrates the viscoelastic shear behavior of materials as a function of frequency, which is the inverse value of time. Short-term properties stimulated at rapid motion using high frequency and long-term properties stimulated at slow motion using low frequency provides time-dependent storage elastic-modulus (G'), viscous loss-modulus (G") and complex viscosity (η^*) to name a few under controlled testing conditions. The hydrogels were cured for 24 h prior to the measurements. To evaluate strain recovery of the fully crosslinked hydrogels, G' and G" was measured under alternating low (1%) and high oscillation strain (100%) conditions at 25 °C and 1 Hz oscillation frequency for seven cycles with 60 s of holding period in each step using 12 mm diameter stainless steel parallel plate geometry.

2.3. Swelling and degradation study

To study the degradation and swelling characteristics of the material, three parallel samples of hydrogels were subjected to acidic, basic, and neutral pH conditions. Briefly, 250 µL gels were prepared in glass vials and the initial weight of the hydrogels was recorded. The gels were then submerged in 1 mL acetate buffer with pH 5, 1 mL 1x PBS with pH 7.4, and 1 mL bicarbonate buffer with pH adjusted to 9.0 using 1 M NaOH, for the acidic, neutral, and basic pH conditions respectively. To observe the swelling and subsequent degradation characteristics of the gels, the gels were weighed, and the buffer was replaced daily for the first four days and subsequently every alternate day until the sample degraded or for a total of 30 days. The remaining weight percentage was calculated by using the formula:

$$\text{Remaining weight}\,\% = \frac{\text{Measured weight}}{\text{Initial Weight}} \times 100$$

Further enzymatic degradation and swelling study of the material was conducted using hyaluronidase at a concentration of 50 U/mL in PBS at pH 7.4. Three parallel samples of 250 µL HA-HA and HA-GA gels were prepared in glass vials of known recorded blank weight, allowed to crosslink for 24 h, weighed with the formed gels, and subsequently submerged in 1 mL hyaluronidase PBS solution. In a similar fashion to the aforementioned swelling and degradation experiment, the hyaluronidase buffer solution was carefully removed prior to measurement every 24 h, the gels were weighed and the enzyme buffer was replaced after each measurement. The degradation weight percentage was calculated using the formula:

$$\text{Remaining weight}\,\% = \frac{\text{Measured weight}}{\text{Initial Weight}} \times 100$$

2.4. Tissue-adhesive tack test

To observe any difference in the adhesive properties of the two hydrogels (HA-HA and HA-GA), a tack adhesion test was performed using a rheometer. We first glued the porcine muscle having the same diameter to that of the geometry (12 mm) to the movable top head of the rheometer and then placed the fully cured 250 µL of HA-HA and HA-GA gels of 2 mm thickness on the bottom plate. Subsequently, the top plate attached with the muscle tissue was placed in contact with the gel with a holding period of 120 s (residence time) during which a constant compressive force of 100 mN was applied to establish a uniform molecular contact between the tissue and the gels. Thereafter, the top plate was pulled up at a constant velocity of 10 µm/*sec* to record the change in axial force (N) with respect to time. The experiments were performed in triplicate at 25 °C. A graph of axial force (N) vs step time was plotted to observe differences between the two hydrogels.

2.5. Anti-oxidant property

To evaluate the free radical scavenging activity of the HA-GA, the DPPH (2,2,1-diphenyl-1-picrylhydrazyl) method was used [31]. Aqueous HA-GA-CDH solution was obtained by dissolution of 1 mg of polymers in 1 mL of deionized water, followed by the addition of an equal volume of a methanol stock solution containing 1 mg of DPPH radical in 12.5 mL methanol. After incubation at 25 °C for 30 min, the absorbance of the resulting solution was measured at 517 nm using a UV−Vis spectrophotometer.

$$\text{The DPPH scavenging activity}(\%) = [(A_0 - A_1)/A_0] \times 100$$

Where, A_0 is the absorbance of blank DPPH solution that was used under the same reaction conditions in the absence of synthesized polymers, and A_1 is the absorbance of DPPH solution in the presence of polymer samples.

2.6. Cell culture

CRL-2429 cells are human fibroblast cells obtained from skin tissue. These cells were cultured in T-75 cell culture flasks in Dulbecco's Modified Eagle Medium (DMEM, Gibco) with 10% fetal bovine serum (Gibco) and 1% Penicillin-Streptomycin as an antibiotic (DMEM complete medium) in a cell culture incubator at 37 °C and 5% CO_2. The medium was changed every alternate day. TrypLE Select (Gibco) was used to detach the cells from the flasks during passaging. Cells were passaged upon reaching around 80% confluency. Cells from passage 18–20 were used for experiments.

THP-1 cells (human monocytic cell line) were cultured in suspension culture in T-25 cell culture flasks in Roswell Park Memorial Institute (RPMI) 1640 medium (Gibco) with 10% fetal bovine serum (FBS) and 1% Penicillin-Streptomycin as an antibiotic (RPMI complete medium) in a cell culture incubator at 37 °C and 5% CO_2. Cells from passage 14–15 were used for experiments.

For isolating murine bone marrow-derived macrophages (BMDM) femurs were collected from mice. After aspirating the cells from the bone marrow, they were cultured in the flasks for two weeks in MEM high glucose medium (Gibco) supplemented with 10% FBS and 10 ng/mL of mCSF. The medium was replenished every 3 days. For the experiments with unactivated phenotypes, these cells were detached using trypsin/EDTA (Gibco) and counted and resuspended in the hydrogels at a concentration of 2×10^6 cells/mL. To induce a proinflammatory activation state, BMDM was treated with 20 ng/mL lipopolysaccharide (LPS) (Invitrogen) and 10 ng/mL INF-γ (R&D systems) for 16 hrs.

Prior to encapsulation, cells were detached from the flasks, centrifuged, and resuspended in complete medium, counted, and the required number of cells was further centrifuged, and the pellets resuspended in HA-GA-CDH or HA-CDH, respectively. Hydrogels were formed by mixing HA-GA-CDH or HA-CDH cell suspension with HA-Ald in equal volumes in cell culture plates. The hydrogels were incubated for 20 min at room temperature to ensure gelation and then 500 µL complete medium was added to each well. The medium was changed every alternate day or as otherwise indicated.

2.7. Live/Dead staining

For live/dead staining, CRL2429 fibroblasts were encapsulated in 200 µL hydrogels at a concentration of 2×10^6 cells/mL in a 48-well plate. The encapsulated cells were cultured for 14 days, with a medium change every alternate day, and cell viability, as well as changes in morphology of the cells, was visualized by LIVE/DEAD staining (Viability/Cytotoxicity Kit for mammalian cells, Molecular Probes, USA) using a fluorescence microscope. To carry out the Live/Dead staining, the medium was aspirated from the wells and the gels were washed with 1x PBS twice. 300 µL Live/Dead staining solution containing 2 µM Calcein AM and 1 µM Ethidium homodimer in 1X PBS was added to the wells and the plates were incubated at 37 °C for 1.5 h. Post-incubation the hydrogels were washed with 1x PBS once and imaged using a 10x objective and a Nikon Eclipse Ts 2 fluorescence microscope. Live/Dead staining was performed on days 1,7 and 14 after the hydrogel formation. Images obtained from the microscope were post-processed using Nikon NIS Viewer and ImageJ software.

2.8. Cell viability under oxidative stress

To observe the effect of the antioxidant property on cellular behavior, CRL-2429 human fibroblast cells were exposed to hydrogen peroxide (H_2O_2) to stimulate free radical formation, along with exposure to the hydrogel material, and subsequently cell viability was quantified using PrestoBlue (Thermofisher) cell viability assays.

For monolayer cultures, cells were plated in 24-well plates at a density of 50,000 cells/well and incubated for 24 h. Post-incubation, 1 mg/mL of HA-CDH and HA-GA-CDH were exposed to the cells. Oxidative stress was induced by adding 200 µM of H_2O_2 along with the materials. The plates were further incubated for 2 days and cell viability was quantified using PrestoBlue cell viability assay.

For 3D cultures, 2×10^6 cells/mL were encapsulated in 200 µL of HA-HA or HA-GA gels in 24 well plates and incubated for 2 days. Post-incubation, 250 µM H_2O_2 was added to the wells to induce oxidative stress. The gels were incubated for 2 days and the medium was replaced. After 2 days, the PrestoBlue cell viability assay was carried out.

2.9. Immunomodulatory property

To observe the immunomodulatory effects of the gels, 4×10^6 THP-1 cells/mL were encapsulated in 200 µL HA-HA or HA-GA gels. The medium was changed every 2 days to account for medium loss due to swelling of gels. Gene expression analysis was performed by RNA extraction, followed by cDNA synthesis from the extracted RNA. The synthesized cDNA was then subjected to a quantitative polymerase chain reaction (qPCR) to quantify the fold change in gene expression levels. RNeasy Plus Mini Kit (Qiagen) was used for RNA extraction. Briefly, the gels were first mechanically disrupted followed by suspension in PBS and centrifuged. Lysis buffer was added to the pellet and the kit protocol was followed. Post-extraction, the RNA samples were stored at −20 °C. cDNA was prepared by following the cDNA synthesis kit (Thermo Fisher Scientific). For qPCR reactions, the cDNA sample was added along with TaqMan Fast Advanced Master Mix (Thermo Fisher Scientific), nuclease-free water (Invitrogen), and TaqMan assay primers and subjected to the reaction process in a Bio-Rad CFX96 Real-time PCR machine as per the manufacturer's protocol. The expression levels of the following genes were analyzed using commercially available TaqMan Gene Expression Assays (Thermo Fisher Scientific): TNF-α (Hs00174128), IL1-β (Hs01555410), IL10 (Hs00961622), IL1RN (Hs00893626), with β-Actin (Hs01060665) as a housekeeping gene.

Murine BMDM was differentiated into a resting phenotype in accordance with the culture conditions outlined above. Cells were then encapsulated in hydrogels at a concentration of 2×10^6 cell/mL and cultured for two weeks, after which gene expression analysis was performed. For the LPS stimulation experiments, the stimulated cells were then encapsulated in the hydrogels and cultured for 3 days, after which gene expression analysis was performed. In each setting RNA was extracted using a commercially available kit (RNeasy Mini kit, Qiagen). cDNA first strand was synthesized following the protocol from the iScript cDNA synthesis kit (BioRad). iQ SYBR Green Supermix was used to prepare the samples for qPCR on a CFX96 instrument from BioRad. The murine primers (sequences in SI) for the qPCR were obtained from Sigma Aldrich, Sweden.

The qPCR data were normalized and analyzed using a comparative quantitation method and data are presented as $\Delta\Delta$Ct method. To unequivocally quantify the immunological response of GA functionalization, we used the HA-HA gel (HA hydrogel without GA) as the normalizing variable. Reference housekeeping gene β-Actin (for the PCR with THP1 cells) and HPRT (for the murine BMDMs) were selected as an internal control for the normalization of qPCR data.

2.10. Multiplex bead-based immunoassays

Bead-based cytokine detection immunoassays from LEGENDplex (BioLegend) were used to identify secreted cytokines following in vitro cell culture. Cell culture supernatants were collected at the respective timepoints and stored at −80 °C before use. The Mouse Macrophage/Microglia Cytokine Panel (BioLegend) was used to detect secreted cytokines as per the manufacturer's instructions. Analyses were performed using LEGENDplex Data Analysis Software (BioLegend) and the cytokines were quantified by comparing samples to a set of standard curves prepared in parallel with supernatant samples.

2.11. In vivo recruitment of immune cells in C57BL/6 mice

Female mice (8–9 weeks old) were injected subcutaneously with 200 µL HA-GA and HA-HA gel on each side of the lower back area. Five days post injection the gels were recovered and digested in 500 µL PBS containing 0.4 mg/mL hyaluronidase (Sigma-Aldrich) and trypsin 1 g/mL (Gibco) for 50 min at 37 °C. The cell suspension was filtered using a 40 µm strainer and centrifuged at 350 g for 5 min at 4 °C. The pellet was resuspended in a cocktail of antibody solution (see below) for 30 min at 4 °C. After a wash with PBS, the cells were centrifuged as above and transferred to FACS tubes. The cells were analyzed using a BD LSR FORTESSA. The data was analyzed using the software Flowjo V 10.8.0. The antibody panel included CD45-PeCy7 1:100, CD11b-PercpCy5.5 1:100, CD36-Pe 1:100, CD86-APC 1:100, MHCII-A700 1:100, CD40-FITC 1:100, live dead marker – Near infrared 1:500). Ethical permission was obtained from the regional ethical committee, Stockholms djurförsöksetiska nämnd (Dnr 9328–2019).

2.12. Statistical analysis

The statistical measurements were achieved by comparing each experimental value with their respective controls (in our case HA-GA was compared with HA-HA). The assessments between the two groups were performed using the student's unpaired T-test and Mann Whitney test as indicated. These tests were performed using GraphPad Prism Software $P<0.05$ was the statistical significance for all tests.

3. Results and discussion

To design the bioactive 3D scaffold we utilized HA, an anionic non-sulfated glycosaminoglycan (GAG), as a base biopolymer. As an immunomodulatory agent we utilized gallic acid (GA), a low molecular weight polyphenol compound occurring naturally in various terrestrial plants including green tea. GA possesses diverse bioactivities such as anti-carcinogenic, anti-mutagenic, and anti-inflammatory properties [32]. We hypothesized that grafting of GA in a HA scaffold would provide antioxidant properties necessary to polarize macrophages into a tissue regenerative phenotype.

Conventionally, GA is conjugated to polysaccharides via ester linkages utilizing the aliphatic hydroxyls on the polymer or by carbodiimide coupling of amine-functionalized GA with the carboxylate residues of the polymer [33,34]. Both these approaches are inefficient, rendering a poor coupling yield. To circumvent this we modified the carboxylate residues of GA to a hydrazide derivative as they are known to undergo proficient EDC coupling owing to a lower pK_a of hydrazides over amines [35]. To achieve this we first transformed the carboxylate groups of GA to methyl ester followed by nucleophilic displacement with aqueous hydrazine (80% solution) to obtain GA-hydrazide in quantitative yields. The hydrazide derivative of GA was characterized by ^{1}H and ^{13}C NMR spectroscopy (Figure S2 and S3 in SI). We have recently shown that compared to hydrogels obtained by $NaIO_4$ oxidation of dopamine conjugated HA, the hydrogel obtained by GA functionalized HA displayed faster oxidation at physiological pH and possess higher tissue adhesive properties [35]. In this study, the GA functionalized HA was grafted with carbodihydrazide (CDH) groups as a biorthogonal moiety that facilitates covalent crosslinking reaction with aldehyde functionalized HA derivative. We have earlier reported that unlike other hydrazone bonds, which are labile, the CDH-derived hydrazones are exceptionally stable under physiological conditions due to their unique delocalized electronic structures [27].

Using this optimized protocol we developed hydrazone crosslinked HA-hydrogels grafted with the GA moiety, in which the degree of GA functionalization was 6% with respect to the disaccharide repeat units (Figure S5 and S6 in SI) and the degree of hydrazone crosslinking was fixed at 10%. For comparison, we used HA gels without GA by using the same hydrazone chemistry with similar levels of crosslinking density using 10 mol% modified HA-Aldehyde (Figure S7 and S8 in SI). A DPPH radical scavenging assay was used as a preliminary assessment of the changes in hydrogel antioxidant property upon the incorporation of gallol moieties. The DPPH reagent underwent a visual change in color from deep purple to deep orange in HA-GA, which is due to the antioxidant property imparted by GA. The UV–Vis spectroscopy measurement of 0.5 mg/mL HA-GA-CDH (75 μM GA grafted on HA-GA-CDH) in presence of DPPH displayed 50% reduction in absorption indicating potent antioxidant properties (Figure S12A in SI).

We performed the rheological evaluation of HA gels (HA-HA) and HA gels with 6% GA (HA-GA gels) by subjecting the gels to amplitude and frequency sweeps. The rheological analyses demonstrated that both HA-HA and HA-GA gels remained stable during the rheological testing and consistently yielded higher storage modulus (G′) values as compared to loss modulus (G′′) (Fig. 2A). For HA-HA gels, a storage modulus, G′, of 995 ± 4 Pa and a loss modulus G′′ of 7 ± 3 Pa was observed, while for HA-GA gels the G′ and G" values were 747 ± 57 and 4 ± 1 Pa, respectively. The tan δ value, which is the ratio between G′ and G′′, yielded significantly less values than 1 (0.0066 and 0.0057 for HA-HA and HA-GA gels, respectively), indicating that the gels were highly elastic in nature. The average mesh size (ξ), which represents the pore size of the gel by considering the distances between the two entanglement points, was calculated to be 16.05 nm and 17.70 nm, respectively, for HA-HA and HA-GA gels. The addition of GA moieties led to a decrease in the storage modulus values, indicating softer gels at the beginning. By using the modulus data, we also calculated the average critical molecular weight between the crosslinks (M_c) using rubber elastic theory that applies to highly elastic gels, which was evident from the tan δ values. M_c values were 39.11 kg mol^{-1} and 44.18 kg mol^{-1} for HA-HA and HA-GA gels, respectively, suggesting that HA-GA gels were softer than HA-HA gels with higher ξ (Table S1).

We next performed swelling studies to investigate the stability of these gels under physiological conditions (pH 7.4) and at acidic conditions (pH 5.0) where the hydrazone crosslinks are susceptible to degradation and at basic pH of 9.0 (Figure S9 in SI). Both HA-HA and HA-GA hydrogels showed rapid initial swelling followed by degradation in acidic buffer (pH 5.0), although the HA-GA gels displayed relatively lower swelling. However, under physiological conditions (pH 7.4) and at pH 9.0, both the gels remained stable.

We were intrigued by the fact that the GA functionalized HA gels did not show any significant swelling or degradation over the period of 25 days under basic or neutral conditions after the initial swelling within 5 days. This observation prompted us to investigate the viscoelastic properties of HA-HA and HA-GA gels at different time points at pH 7.4 to decipher the role of GA in inducing this characteristic. Fascinatingly, we observed matrix stiffening in HA-GA hydrogels at day 2 compared to day 0 when immersed in PBS at pH 7.4 (Fig. 2B). Thereafter, the HA-GA gels exhibited exceptionally stable storage modulus compared to HA-HA hydrogels until day 21, whose storage modulus slowly deteriorated until day 15 and then underwent rapid loss by day 21 (Fig. 2B). This clearly suggests that the grafting of GA in HA gels promote the formation of secondary network that stabilizes the gel and prevent excessive swelling (Table S2). We believe this is attributed to the unique capability of the gallol moiety to undergo oxidation that generates radicals and undergo intermolecular dimerization [35]. Such secondary stabilization decreases the segmental mobility of the polymer chains and reduces the pore size, favoring a stiffer and stable matrix formation.

To determine the injectability of these chemically cross-linked hydrogels we determined the flow behavior (viscosity) at room temperature (Figure S10) by continuously increasing the shear rate up to 10 s^{-1}. Both the HA-HA and HA-GA hydrogels displayed a rapid decline in the viscosity upon application of increasing shear rate (0.01 to 10 s^{-1}), suggesting their injectability. We further ascertained the shear-thinning characteristics of these gels by estimating the viscosity recovery by performing a dynamic experiment applying a periodic low (0.01 s^{-1}) and high shear rate (10 s^{-1}) to the hydrogel samples (seven cycles; Figure S11 in SI). Both the hydrogels recovered their initial viscosity when the shear rate was periodically lowered. We also tested the dynamic strain recovery properties of these hydrogels (Fig. 2C and 2D). At low strain (1%), both the hydrogels displayed higher storage modulus, and with increasing strain (100%) the storage modulus was reduced while loss modulus increased in HA-GA hydrogels, while they were similar in case of HA-HA gels. Upon withdrawal of the high strain both hydrogels recovered their initial storage modulus, suggesting the dynamic nature of the hydrogel chemistry.

We next performed tissue adhesion tack tests using a rheometer in order to investigate the tissue adhesive properties using porcine muscle tissue as a model. Notably, both HA-HA and HA-GA gels showed tissue-adhesive properties (Fig. 2E). However, HA-GA had significantly greater adhesion to the wet muscle tissue, as a greater negative force was required to induce cohesive failure between the top plate and the gel.

To further prove the gallol-mediated secondary network formation in the HA-GA hydrogels we performed an enzymatic degrada-

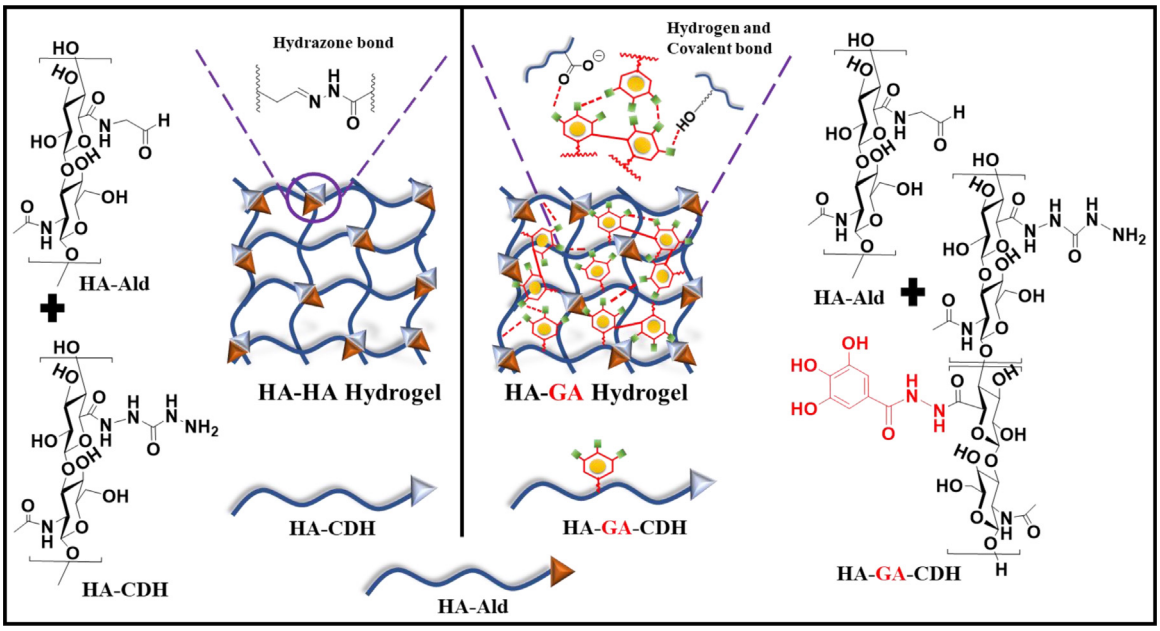

Fig. 1. Schematic representation of the formation of hydrazone crosslinked HA-HA and hydrazone and gallol crosslinked interpenetrating HA-GA hydrogel.

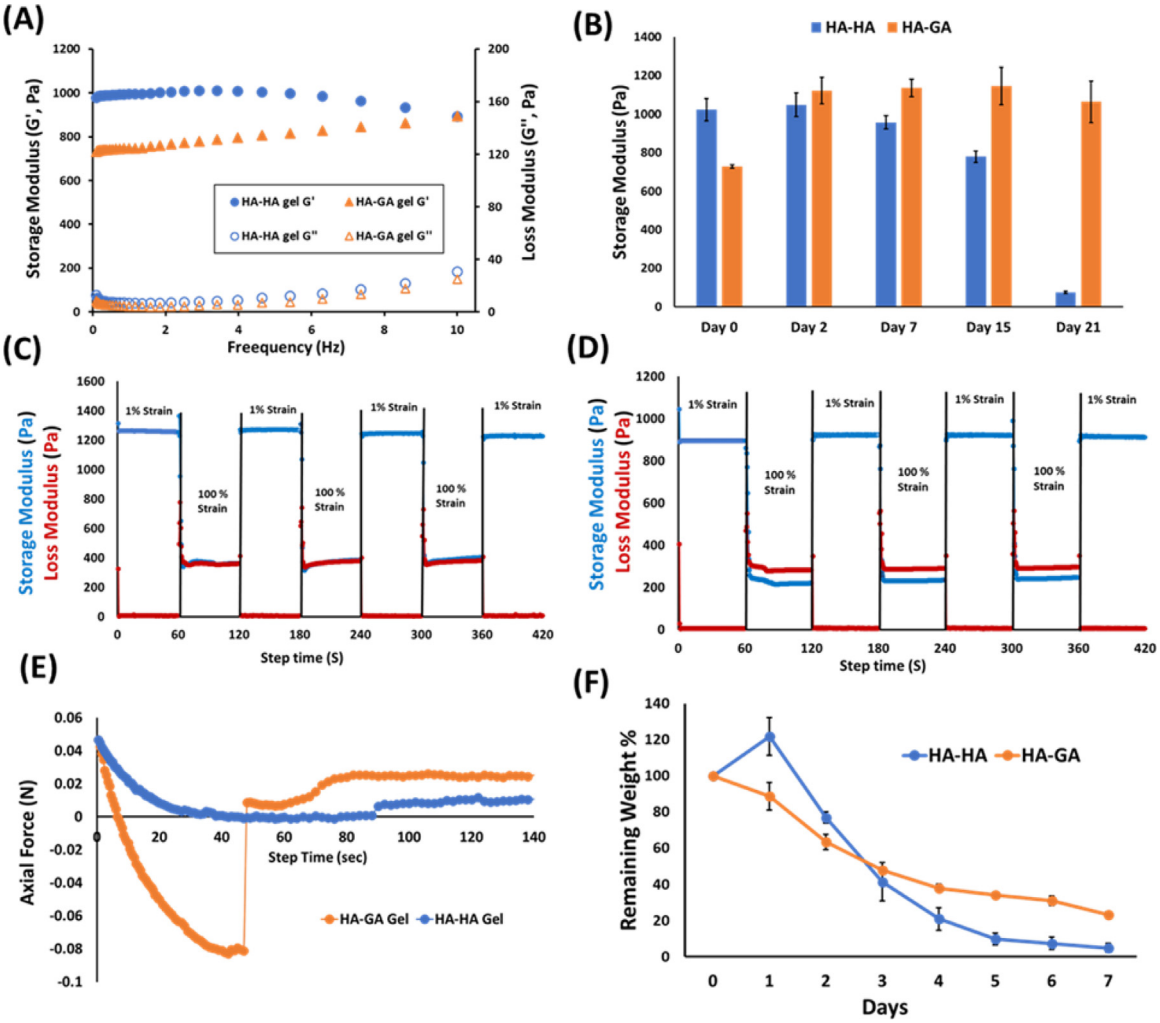

Fig. 2. (A) Rheological measurements obtained from frequency sweep for 250 µL HA-HA and HA-GA hydrogels ($n = 3$). (B) Rheological measurements of HA-HA and HA-GA hydrogels (250 µL, $n = 3$) immersed in PBS buffer (pH 7.40). Dynamic strain recovery of a (C) HA-HA, and (D) HA-GA hydrogel undergoing cyclic deformation of 1% (low) and 100% (high) strain at 1 Hz with G' (blue line) and G'' (red line). (E) Measurement of tissue adhesion force of the two hydrogels by rheological tack adhesion test (250 µL gels). (F) Degradation profiles of HA-HA and HA-GA hydrogels (250 µL, $n = 3$) in neutral PBS (pH 7.4) buffer containing 50 U/mL hyaluronidase. (For interpretation of the references to colour in this figure legend, the reader is referred to the web version of this article.)

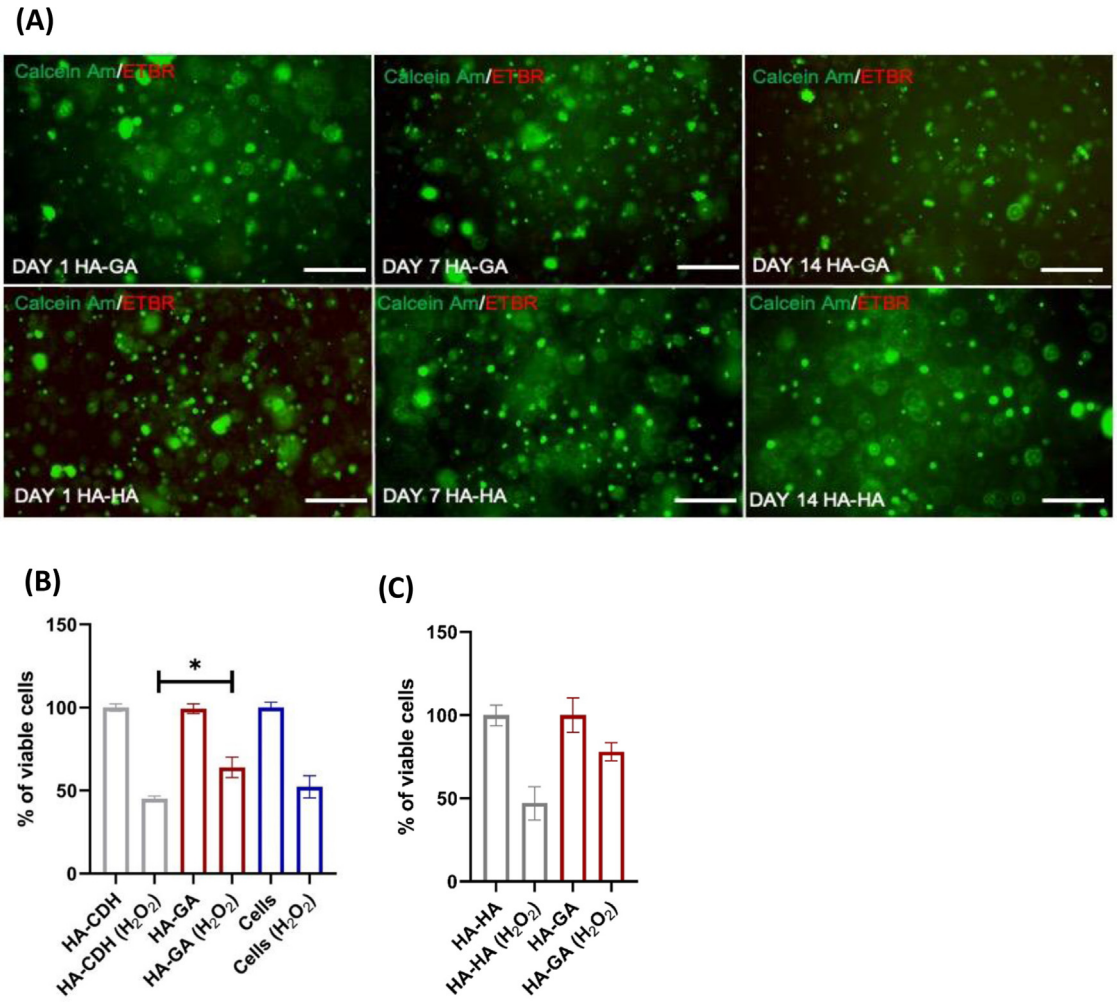

Fig. 3. (A) LIVE/DEAD staining of CRL2429 fibroblasts encapsulated inside hydrogels on 1, 7, and 14 days of culture. Cells stained in green (Calcein AM) represent live cells while cells stained in red (EtBr) represent dead cells. (Scale bar = 500 μm, Cell density = 2×10^6/mL). (B) 2D monolayer and (C) 3D encapsulated cells Presto Blue viability assays showing the antioxidant effect of GA moieties on CRL2429 cells during induced oxidative stress. HA-GA improves cell viability during oxidative stress in (B) monolayer and (C) 3D cultures. (Cell density = 5×10^4 cells/well for 2D ($n = 6$) and 2×10^6/mL for 3D cultures, ($n = 3$)). Statistical analysis used the Mann-Whitney Test $^*P<0.05$. (For interpretation of the references to colour in this figure legend, the reader is referred to the web version of this article.)

tion study in the presence of hyaluronidase in PBS at pH 7.4. Enzymatically, the HA-GA gels illustrated slower degradation in the presence of hyaluronidase than did the HA-HA gels, especially after day 2 (Fig. 2F). Conversely, the HA-HA gels initially swelled and then degraded at a faster rate than did HA-GA in the presence of hyaluronidase. The additional GA-mediated secondary crosslinking network along with the primary hydrazone network in the HA-GA hydrogel thus limits the hydrogel swelling and restricts the enzymatic degradation by bulk erosion, yet promotes degradation by surface erosion.

We next evaluated the biocompatibility of the materials using in vitro studies. We first encapsulated CRL2429 fibroblasts in both HA-HA and the HA-GA hydrogels and evaluated cell viability inside the hydrogels using live/dead staining. We observed that after 14 days in culture the CRL2429 fibroblasts were viable in both gels (Fig. 3A). To further confirm that primary cells are also viable in our hydrogels, we cultured the human bone marrow-derived mesenchymal stem cells (MSCs) and BMDMs (M0) in the two gels and performed live/dead staining. Interestingly, we did not observe significant cell death at the respective time points with both the cell types (Figure S13A & S13B in SI). To corroborate the viability and proliferation of cells (MSCs) in our hydrogels, we measured the DNA content of the cells from the respective hydrogels using the CyQuant cell proliferation kit at days 1,7,14 and 21, respectively. These experiments revealed that the cells were viable and proliferating from day 1 to day 21 in HA-HA gels. In the case of HA-GA hydrogels, we recorded limited cell proliferation between days 1 and 14 and a subsequent increase in the proliferation up to day 21 (Figure S13C in SI). The reduction of the cell proliferation could be attributed to the effect of the gallol on MSC proliferation [36].

To ascertain the antioxidant properties of the gallol-modified HA we first incubated the individual hydrogel components (HA-CDH and HA-GA-CDH) with the CRL2429 cells in the presence or absence of hydrogen peroxide (H_2O_2). Cells cultured in 2D without incubating with any hydrogel components (cultured in the presence or absence of H_2O_2) were used as a control group. As expected, we observed a reduction in cell viability (~50% reduction) when the cells were exposed to 200 μM H_2O_2. When HA-CDH (1 mg/mL) was added to the cells we observed a ~55% reduction of cell viability in the H_2O_2-treated cells compared to the untreated cells. Interestingly, when the cells were incubated within HA-GA (1 mg/mL), there was only ~36% reduction in the cell viability when exposed to 200 μM H_2O_2 (Fig. 3B). This clearly suggests that the GA moiety in the HA-GA polymer contributes to the radical scavenging property.

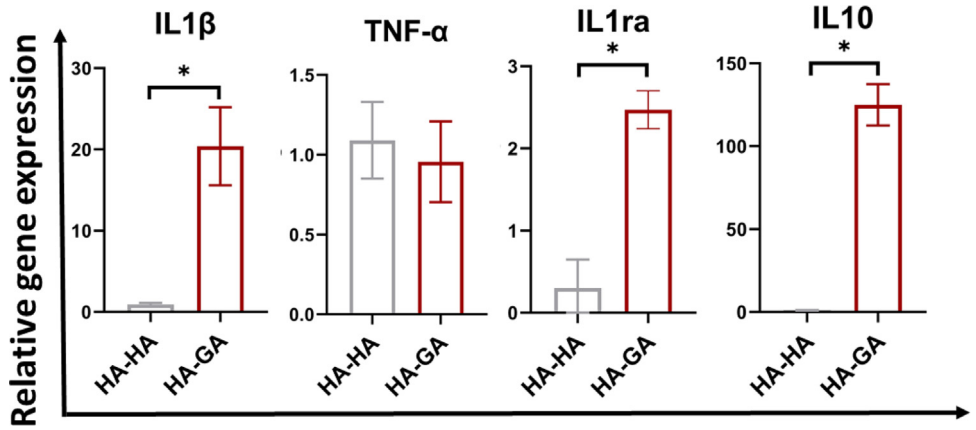

Fig. 4. Gene expression analysis of pro-inflammatory markers TNF-α and IL-1β and anti-inflammatory markers IL-10 and IL-1ra in THP-1 cells encapsulated in HA-GA hydrogels for 8 days in basal medium, as compared to HA-HA gels. Expression of anti-inflammatory markers was increased in HA-GA gels as compared to HA-HA gels, suggesting increased immunosuppressive polarization (200 µL gels. THP-1 density = 4×10^6/mL, $n = 6$). Statistics used Mann-Whitney Test $^*P<0.05$. (For interpretation of the references to colour in this figure legend, the reader is referred to the web version of this article.)

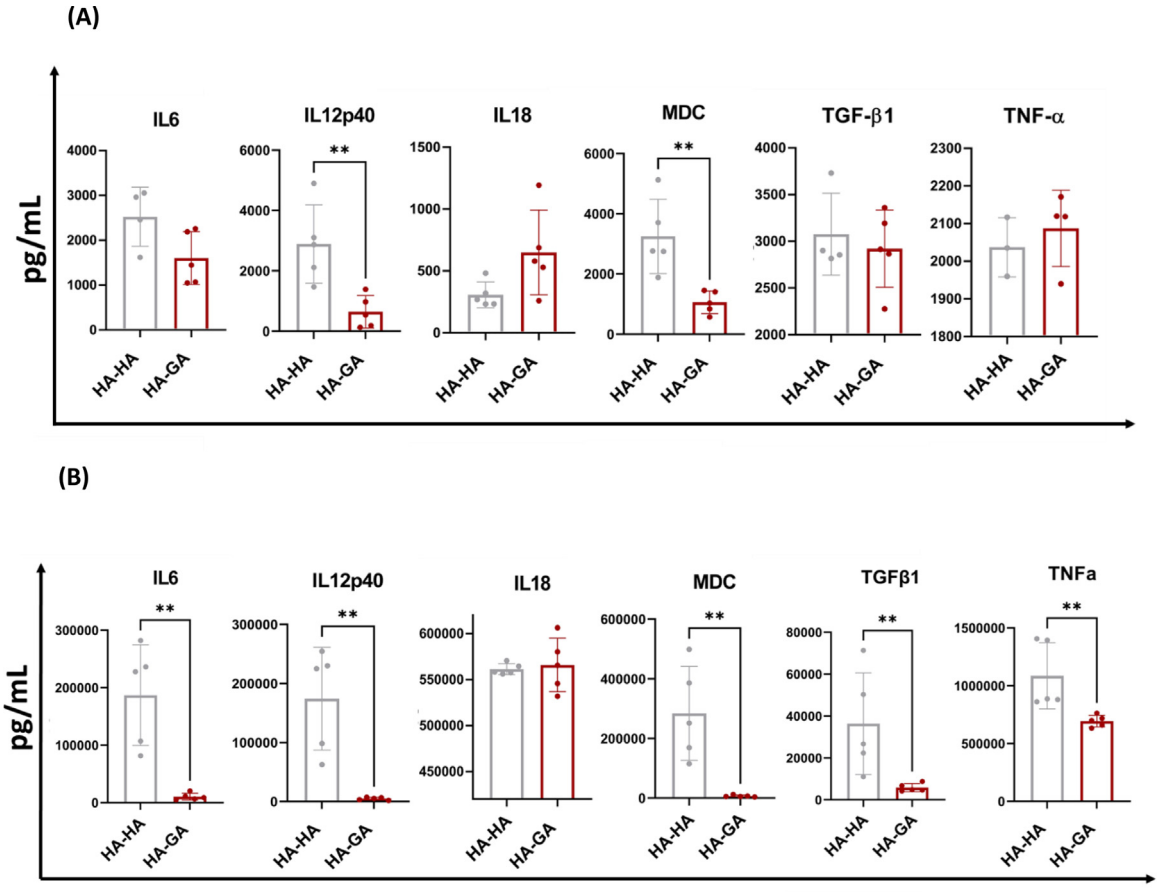

Fig. 5. Cytokine release in the medium by the primary murine BMDM cells analyzed by capture bead assay on (A) day 1 and (B) day 10. Statistical analysis done by Mann-Whitney Test using GraphPad Prism. $^{**}P<0.01$ (C) Cytokine mRNA levels produced by the BMDM cells as determined by qRT-PCR when encapsulated within HA-HA and HA-GA gels ($n = 5$) for 14 days. Statistical analysis using student T-test $^*P<0.05$.

To validate the antioxidant properties of the HA-GA hydrogels we performed 3D cellular oxidative stress measurement experiments. We encapsulated the CRL2429 fibroblasts in HA-HA and HA-GA gels and induced oxidative stress by exposing the system to 250 µM H_2O_2 for 48 h. The cells cultured in HA-HA gels displayed significant oxidative stress upon exposure to H_2O_2 and their viability was drastically reduced to 50% after 48 h in culture. As anticipated, the cells encapsulated in the HA-GA gels displayed higher cell viability (~78%) upon exposure to H_2O_2 (Fig. 3C and Figure S12B). These experiments suggest that the GA component in the hydrogel network shielded the encapsulated cells from oxidative stress by scavenging free radicals induced by the addition of H_2O_2.

As blood-derived monocytes are early responders to inflammation and injury that can differentiate into activated phenotypes we investigated if our HA-GA gels provided the necessary cues for the differentiation of monocytes to M1 or M2 macrophages, respec-

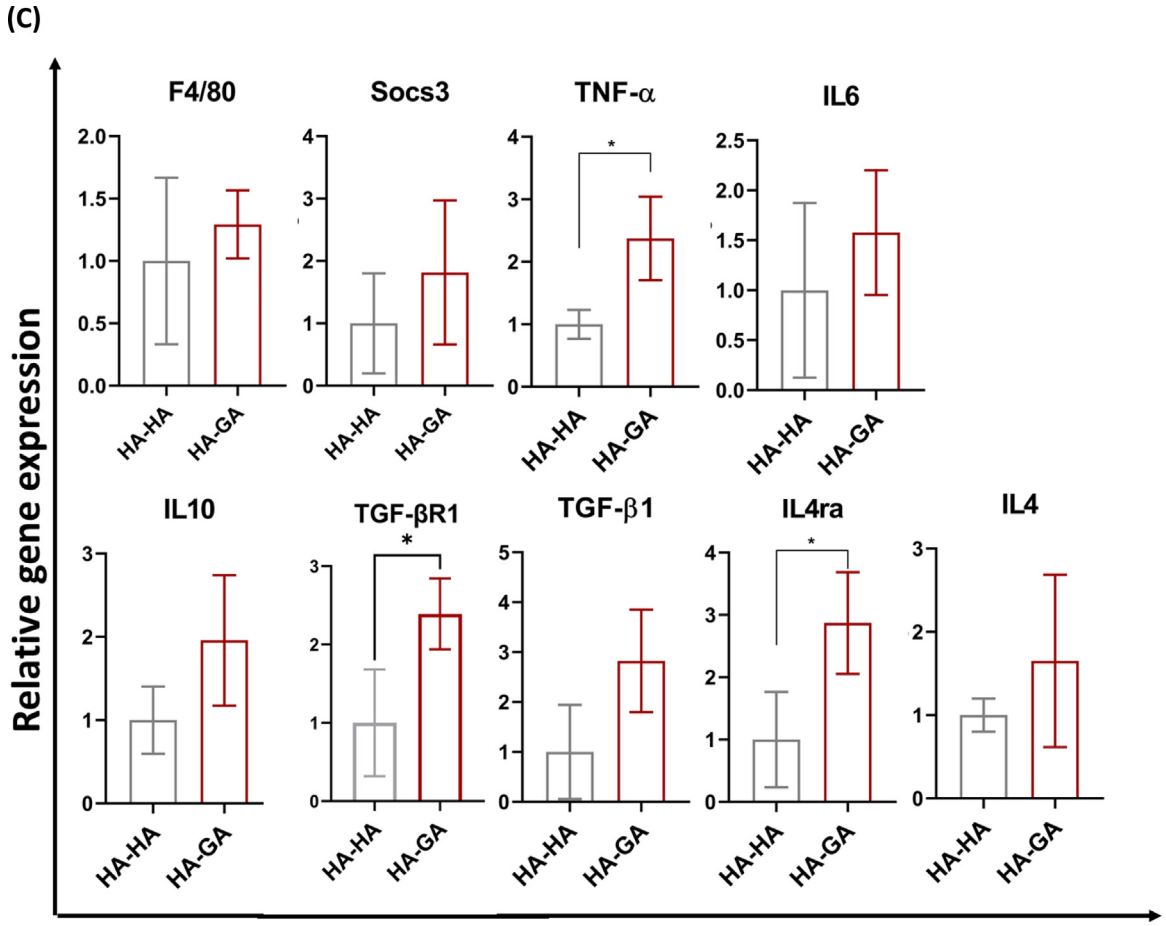

Fig. 5. Continued

tively (Fig. 4). For this purpose, we encapsulated human monocyte THP-1 cells in HA-HA and HA-GA gels without the addition of any immunomodulatory agents or differentiation factors. After 8 days in culture we observed that relative to the HA-HA gels, cells cultured in HA-GA gels exhibited ~125-fold higher expression of IL-10 and ~2.5-fold increase in IL-1ra as quantified by qRT-PCR. The higher expression of IL-10 and IL-1ra indicates that the macrophages had become preferably polarized towards an immunosuppressive M2 phenotype in HA-GA gels [37]. Interestingly, we also observed a ~20-fold increase in IL-1β, a pro-inflammatory cytokine. It is important to consider that it is the net sum of inflammatory genes that determine the final macrophage activation phenotype, so the co-expression of both pro-inflammatory and immunosuppressive markers is expected. Immunosuppressive macrophages are known to mitigate tissue damage and to contribute to the recovery from conditions such as spinal cord injury and myocardial ischemia [38,39]. Furthermore, we believe that the substantial amount of IL-10 produced by these cells inhibits the differentiation of neighboring cells into pro-inflammatory activated macrophages by repressing the pro-inflammatory genes via the IL-10/STAT3 pathway [40] and thereby allowing the macrophage population to be self-regulating [41] which could be useful in reducing inflammation and could facilitate wound healing and tissue regeneration.

To further substantiate our observation that HA-GA gels polarize macrophages towards an immunosuppressive profile, we conducted further experiments by encapsulating murine bone marrow-derived primary macrophages (BMDM) in their resting state (M0 macrophage) within the HA-GA gels for 10 days. The BMDM cells used in this study were isolated and cultured following a standard protocol [42]. The conditioned media was collected on day 1 and day 10 and analyzed using a multiplex bead-based assay (LEGENDplex from Biolegend) (Fig. 5A>, 5B). We observed that at day 1 the cells cultured in the HA-GA gels produced lower levels of pro-inflammatory cytokines such as IL-6 (1.6 $\pm$ 0.5 ng/mL in HA-GA vs 2.5 $\pm$ 0.5 ng/mL in HA-HA), IL-12p40 (0.6 $\pm$ 0.4 ng/mL in HA-GA vs 3 $\pm$ 1 ng/mL in HA-HA) and MDC (1 $\pm$ 0.3 ng/mL in HA-GA vs 3 $\pm$ 1 ng/mL in HA-HA) when compared to the HA-HA gels. Interestingly, TGF-β (3 $\pm$ 0.3 ng/mL) and TNF-α (2 $\pm$ 1 ng/mL) cytokine release in the day 1 HA-GA gels were similar to that of the HA-HA gels (TGF-β – 3 $\pm$ 0.3 ng/mL; TNF-α – 2 $\pm$ 0.8 ng/mL). When the conditioned media obtained after 10 days of culture was analyzed, a similar trend was observed whereby the HA-GA gels had released significantly lower amounts of pro-inflammatory cytokines when compared to the HA-HA gels. Specifically, IL-6 (187 $\pm$ 28 ng/mL in HA-HA vs 104 $\pm$ 5 ng/mL in HA-GA), IL-12p40 (174 $\pm$ 78 ng/mL in HA-HA vs 5 $\pm$ 2 ng/mL in HA-GA), MDC (284 $\pm$ 140 ng/mL in HA-HA vs 7 $\pm$ 3 ng/mL in HA-GA) and TNF-α (1086 $\pm$ 257 ng/mL in HA-HA vs 695 $\pm$ 45 ng/mL in HA-GA) expression were significantly lower in the HA-GA gels, while IL-18 released by both the gels was at similar levels. Unexpectedly, TGF-β was less abundant in the HA-GA gels (6 $\pm$ 2 ng/mL) compared to the HA-HA gels (36 $\pm$ 22 ng/mL). These results indicate that HA-GA gels have the potential to drive BMDM towards a less inflammatory phenotype than do the HA-HA gels.

To further quantitatively assess the immunosuppressive characteristics, we analyzed mRNA expression of the pro-inflammatory and anti-inflammatory genes. For this purpose, BMDM cells (M0

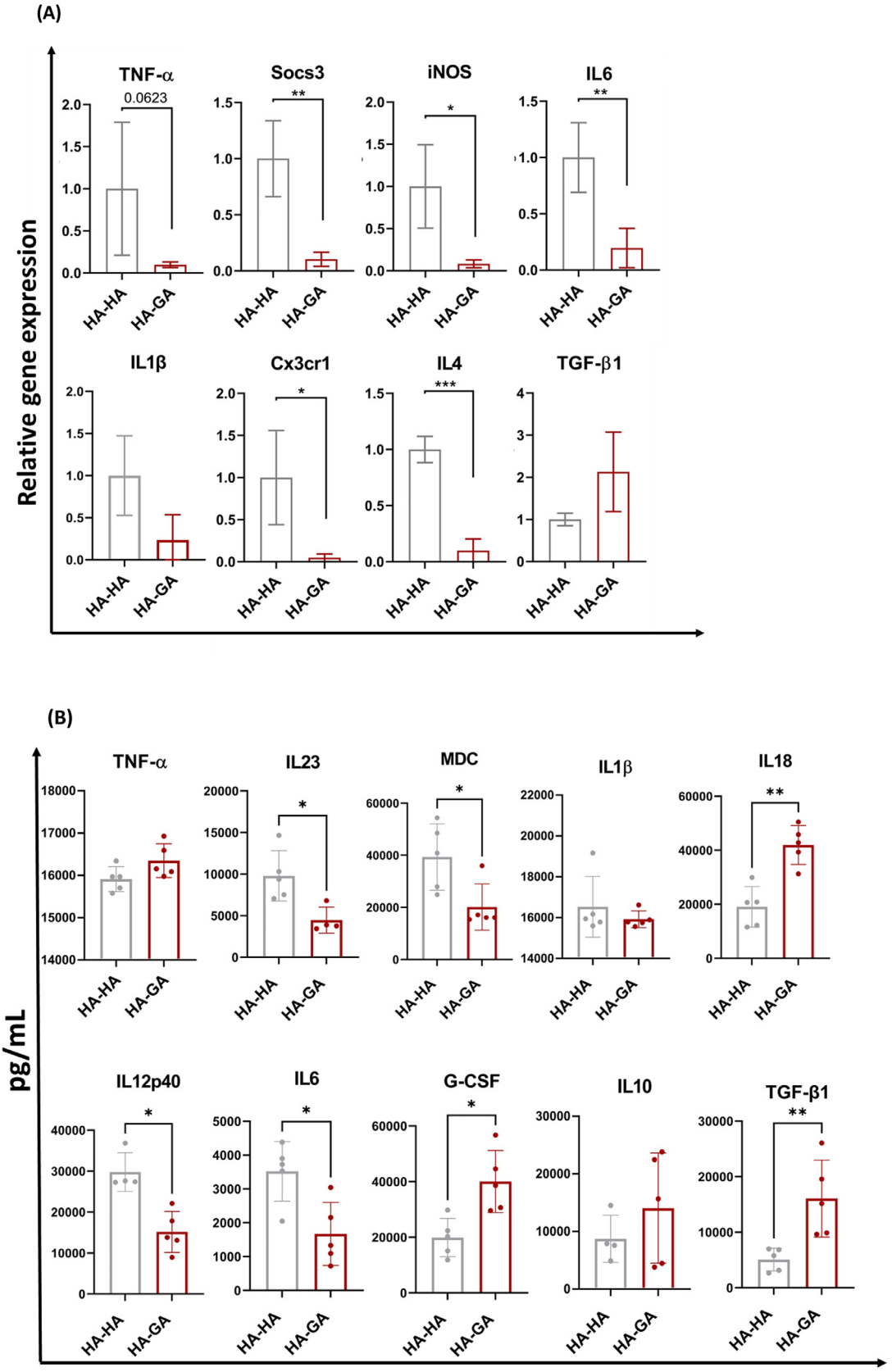

Fig. 6. (A) Primary murine BMDM cells were stimulated with LPS/IFNγ for 16 h and then encapsulated in HA-HA and HA-GA gels ($n = 4$) for 3 days. The expression of different inflammatory markers was determined by qRT-PCR. Statistics done by T-test using GraphPad Prism. $^{*}P<0.05$, $^{**}P<0.005$, $^{***}P<0.001$ (B) Cytokine present in the medium detected by multiplex bead-based assay after 3 days. Statistical analysis used Mann-Whitney Test. $^{*}P<0.05$, $^{**}P<0.01$.

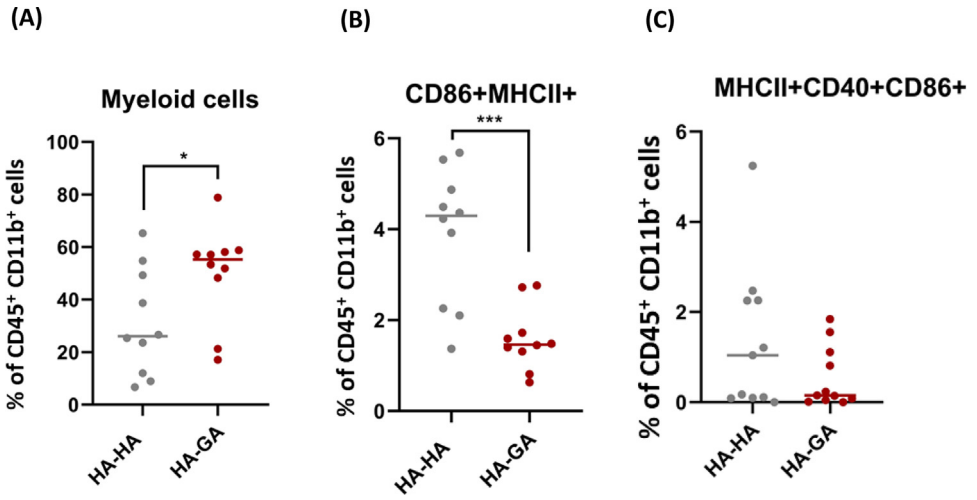

Fig. 7. Flow cytometric analysis of the cells recruited into the HA-HA and the HA-GA hydrogels when implanted subcutaneously in C57L/B6 mice. The hydrogels were excised and the cells recovered after dissolution of the hydrogels using hyaluronidase enzyme. The cells were then stained with CD86, MHCII, CD40 and CD45 antibodies and analyzed using flow cytometry. Statistics used student T-test. $^{*}P<0.05$, $^{**}P<0.005$, $^{***}P<0.0005$. (For interpretation of the references to colour in this figure legend, the reader is referred to the web version of this article.)

state) were encapsulated in the HA-HA and HA-GA hydrogels and cultured for 14 days. RNA was extracted from these gels and the expression of pro-and anti-inflammatory genes was quantified by qRT-PCR (Fig. 5C). We observed that the resting M0 macrophages differentiated into mature macrophages as evidenced by the expression of F4/80, a murine macrophage marker [43]. Interestingly, we observed an upregulation of anti-inflammatory genes, namely il10 (∼2-fold), tgfb-1 (∼3-fold), il4 (∼1.5-fold), il4ra (∼ 3-fold), and tgfb-r1 (∼2.5-fold), when compared to cells encapsulated in HA-HA gels (Fig. 6). Similar to the previous study with the THP1 cells, we also observed an upregulation of a few pro-inflammatory genes such as socs3 (∼2-fold), il6 (∼1.5-fold), and tnfa (∼2.5-fold) by the BMDM cells relative to cells encapsulated in the HA-HA gels. These results concord with our hypothesis that the covalent grafting of GA to the HA backbone acts as a cue to polarize macrophages towards an immunosuppressive phenotype [32]. The expression of the proinflammatory markers (SOCS3, IL6, and TNF-α) could be attributed to the flexible phenotypic paradigms of the macrophages [11]. There have also been reports suggesting that the temporality and responsiveness of macrophage functions necessitate this flexibility, with M2- activated macrophages being able to display M1-like features or to repolarize completely [44].

Although the results with the M0 macrophages indicated promising immunosuppression, the extent of this characteristic was not very clear. We therefore tested the immunosuppressive propensity of HA-GA gels by encapsulating proinflammatory BMDM cells (that were pre-stimulated with lipopolysaccharide (LPS) (10 ng/mL) and IFNγ (20 ng/mL) and estimated the gene expression after 3 days. As anticipated, we observed a significant decrease in expression of proinflammatory genes such as socs3, iNOS, and il6 (Fig. 6A), and a non-significant decrease in il-1β and tnf-α expression, which are hallmarks of pro-inflammatory M1 macrophages [16], in the HA-GA gels relative to the HA-HA gels. Interestingly, we also observed an increase in the expression of tgf-β1 in the HA-GA gels when compared to in HA-HA gels. However, we also observed a decrease in IL4 in the HA-GA gels with respect to the HA-HA gels. A significant decrease in expression levels of chemokine-derived cx3cr1 was also observed in the HA-GA gels. It has been reported that macrophages with low levels of cx3cr1 have the ability to express both pro-inflammatory and anti-inflammatory markers [45] and could be vital in the early and late stages of wound healing and repair in spinal cord injuries [46].

To further validate the immunosuppressive properties of the HA-GA gels, we estimated the amounts of the cytokines released by the pro-inflammatory BMDM cells upon encapsulation within the HA-HA or HA-GA gels after 3 days of culture following a multiplex bead-based assay (Fig. 6B). Interestingly, corroborating the qRT-PCR study we observed a significant reduction in most of the pro-inflammatory cytokines released by these cells in the HA-GA gels compared to in the HA-HA gels. Specifically, pro-inflammatory cytokines such as IL-23 (10 ± 3 ng/mL in HA-HA vs 4.5 ± 2 ng/mL in HA-GA), IL-6 (3.6 ± 1 ng/mL in HA-HA vs 1.7 ± 1 ng/mL in HA-GA), macrophage derived chemokine (MDC; 39 ± 12 ng/mL in HA-HA vs 20 ± 8 ng/mL in HA-GA) and IL-12p40 (30 ± 4 ng/mL in HA-HA vs 15 ± 4 ng/mL in HA-GA) were markedly decreased in the HA-GA gels compared to in the HA-HA gels. However, some pro-inflammatory cytokines such as TNF-α (16 ± 0.3 ng/mL in HA-HA vs 16 ± 0.4 ng/mL in HA-GA) and IL-18 (19 ± 7 ng/mL in HA-HA vs 42 ± 7 ng/mL in HA-GA) were upregulated in the HA-GA gels. Interestingly, we also observed that BMDM cells upregulated the production of anti-inflammatory cytokines when encapsulated in the HA-GA gels such as granulocyte colony stimulating factors (20 ± 7 ng/mL in HA-HA vs 40 ± 11 ng/mL in HA-GA), IL-10 (9 ± 4 ng/mL in HA-HA vs 14 ± 9 ng/mL in HA-GA) and TGF-β (5 ± 2 ng/mL in HA-HA vs 16 ± 7 ng/mL in HA-GA). The qRT-PCR together with the cytokine multiplex bead-based assay thus clearly suggest that the HA-GA gels predominantly possesses an immunosuppressive characteristic compared to the HA-HA gels.

Finally, to unequivocally validate the immunosuppressive characteristics of the HA-GA gels relative to the HA-HA gels we subcutaneously implanted the gels into healthy naive mice and evaluated the type of immune cells that infiltrated these gels after 5 days or 10 days of implantation. In order to minimize the variations between the groups, the HA-HA and HA-GA hydrogels were injected at two different subcutaneous sites in the same animals. Five days post implantation these hydrogels were recovered and the immune cells that infiltrated within the gels were harvested, stained with antibodies and analyzed by flow cytometry. Interestingly, we observed that the HA-GA cells attracted more myeloid cells ($CD45^{+}CD11^{+}$) relative to the HA-HA gels, clearly demonstrating differential properties (Fig. 7A and S14A in SI). However, when we examined the infiltrating cells for the pro-inflammatory markers CD86 and MHCII (Major Histocompatibility factor) [47] and CD40 [48,49] we noted that the percentage of cells

expressing $CD86^{+}MHCII^{+}$ was significantly higher in the HA-HA hydrogels compared to in the HA-GA hydrogels. (Fig. 7B and S14B in SI) Similar trends was observed for the $CD86^{+}MHCII^{+}CD40^{+}$ expressing myeloid cells (Fig. 7C) although the percentage of the myeloid cells remained the same in both groups. We believe that the lower expression of $CD86^{+}$ on cells in the HA-GA gels could be due to the intrinsic ability of the HA-GA gels to stimulate the infiltrating macrophages to secrete more IL-10, as we observed in the in vitro studies (Fig. 4, 5C & 6B). The presence of $CD40^{+}$cells in the HA-GA gels and the ability of the HA-GA gels to stimulate the cells to produce IL-10 could help in the reduction in the population of the proinflammatory $CD86^{+}$ $MHCII^{+}$cells [50]. Fascinatingly, when we analyzed the 10 days old implanted gels, we found that the HA-HA gels were intact, however, the HA-GA gels were completely resorbed. This unique degradation profile of HA-GA gels could be attributed to the higher number of M2 macrophages in the infiltrating myeloid cell population. Such fast degradation was observed after intradermal implantation of collagen matrix in mice that was attributed to the M2-like macrophages [51], which dramatically enhances the capacity to turnover extracellular matrix by an intracellular pathway. This was also confirmed by another study in which IL-4-containing implants display a distinct population of macrophages with an M2-like phenotype, yielding significant proteolytic activity, decreased fibrotic capsule deposition and improved peri–implant tissue quality [52]. These in-vitro and in-vivo results confirm our hypothesis that the HA-GA gels are more immunosuppressive when compared to the HA-HA gels and indicate that they could be utilized in the treatment of specific inflammatory diseases.

4. Conclusion

Undesired immune reaction to the implanted biomaterial is the major bottleneck for successful clinical translation of regenerative medicine and cell-based therapies. To address this, we have designed an innovative GA functionalized HA-based extracellular matrix mimetic (HA-GA) hydrogel that displays superior antioxidant and tissue-adhesive properties. The secondary network due to the presence of GA moiety in the HA-GA gels rendered an extremely stable hydrogel formation without excessive swelling. In addition, these scaffolds displayed a unique capability to differentiate monocytes to an immunosuppressive phenotype. Fibroblasts encapsulated inside these HA-GA gels were protected from oxidative stress. Our study clearly suggests that GA functionalized gels display radical scavenging activity and promote polarization of macrophages into an immunosuppressive phenotype have great potential to be used as scaffolds for cell-based therapies. The ability of the HA-GA gels to suppress the major pro-inflammatory genes and an increase in the TGF-β and IL-10 suggests that these hydrogels may be a valuable tool for tissue engineering applications, especially for wound healing during which suppression of inflammation is crucial [53] (Fig. 1).

Declaration of Competing Interest

The authors declare that they have no known competing financial interests or personal relationships that could have appeared to influence the work reported in this paper.

The authors declare no conflict of interest.

Acknowledgements

SS thanks the European Union's Horizon 2020 Marie Sklodowska-Curie Grant Program (Agreement No. 713645) for the financial support. The authors would also like to thank Dr. Irene Benito Cuesta from the Applied Immunology and Immunotherapy, Department of Clinical Neuroscience, Karolinska Institutet, Stockholm for assisting in the in vivo studies.

Supplementary materials

Supplementary material associated with this article can be found, in the online version, at doi:10.1016/j.actbio.2022.01.048.

References

[1] G.S. Hussey, J.L. Dziki, S.F. Badylak, Extracellular matrix-based materials for regenerative medicine, Nat. Rev. Mater. 3 (2018) 159–173, doi:10.1038/s41578-018-0023-x.
[2] J. Nicolas, S. Magli, L. Rabbachin, S. Sampaolesi, F. Nicotra, L. Russo, 3D Extracellular Matrix Mimics: fundamental Concepts and Role of Materials Chemistry to Influence Stem Cell Fate, Biomacromolecules 21 (2020) 1968–1994, doi:10.1021/acs.biomac.0c00045.
[3] S. Raveendran, A.K. Rochani, T. Maekawa, D.S. Kumar, Smart carriers and nanohealers: a nanomedical insight on natural polymers, Materials (Basel) 10 (2017), doi:10.3390/ma10080929.
[4] B.M. Holzapfel, J.C. Reichert, J.T. Schantz, U. Gbureck, L. Rackwitz, U. Nöth, F. Jakob, M. Rudert, J. Groll, D.W. Hutmacher, How smart do biomaterials need to be? A translational science and clinical point of view, Adv. Drug Deliv. Rev. 65 (2013) 581–603, doi:10.1016/j.addr.2012.07.009.
[5] C.E. Witherel, D. Abebayehu, T.H. Barker, K.L. Spiller, Macrophage and Fibroblast Interactions in Biomaterial-Mediated Fibrosis, Adv. Healthc. Mater. 8 (2019) 1–16, doi:10.1002/adhm.201801451.
[6] D.F. Williams, Biocompatibility pathways: biomaterials-induced sterile inflammation, mechanotransduction, and principles of biocompatibility control, ACS Biomater. Sci. Eng. 3 (2017) 2–35, doi:10.1021/acsbiomaterials.6b00607.
[7] I.M. Adjei, G. Plumton, B. Sharma, Oxidative Stress and Biomaterials: the Inflammatory Link, in: Oxidative Stress Biomater., Elsevier, 2016, pp. 89–115, doi:10.1016/B978-0-12-803269-5.00004-8.
[8] J. Lee, Y.S. Cho, H. Jung, I. Choi, Pharmacological regulation of oxidative stress in stem cells, Oxid. Med. Cell. Longev. (2018) 2018, doi:10.1155/2018/4081890.
[9] R. Sridharan, A.R. Cameron, D.J. Kelly, C.J. Kearney, F.J. O'Brien, Biomaterial based modulation of macrophage polarization: a review and suggested design principles, Mater. Today. 18 (2015) 313–325, doi:10.1016/j.mattod.2015.01.019.
[10] P. Italiani, D. Boraschi, From monocytes to M1/M2 macrophages: phenotypical vs. functional differentiation, Front. Immunol. 5 (2014) 514, doi:10.3389/fimmu.2014.00514.
[11] D.M. Mosser, J.P. Edwards, Exploring the full spectrum of macrophage activation, Nat. Rev. Immunol. 8 (2008) 958–969, doi:10.1038/nri2448.
[12] M.M. Alvarez, J.C. Liu, G. Trujillo-de Santiago, B.H. Cha, A. Vishwakarma, A.M. Ghaemmaghami, A. Khademhosseini, Delivery strategies to control inflammatory response: modulating M1–M2 polarization in tissue engineering applications, J. Control. Release. 240 (2016) 349–363, doi:10.1016/j.jconrel.2016.01.026.
[13] Z. Julier, A.J. Park, P.S. Briquez, M.M. Martino, Promoting tissue regeneration by modulating the immune system, Acta Biomater 53 (2017) 13–28, doi:10.1016/j.actbio.2017.01.056.
[14] R.A. Harris, Spatial, temporal, and functional aspects of macrophages during "The good, the bad, and the ugly" phases of inflammation, Front. Immunol. 5 (2014) 3–6, doi:10.3389/fimmu.2014.00612.
[15] R. Parsa, H. Lund, I. Tosevski, X.-M. Zhang, U. Malipiero, J. Beckervordersandforth, D. Merkler, M. Prinz, A. Gyllenberg, T. James, A. Warnecke, J. Hillert, L. Alfredsson, I. Kockum, T. Olsson, A. Fontana, T. Suter, R.A. Harris, TGFβ regulates persistent neuroinflammation by controlling Th1 polarization and ROS production via monocyte-derived dendritic cells, Glia 64 (2016) 1925–1937, doi:10.1002/glia.23033.
[16] F.O. Martinez, S. Gordon, The M1 and M2 paradigm of macrophage activation: time for reassessment, F1000Prime Rep 6 (2014), doi:10.12703/P6-13.
[17] D.P. Vasconcelos, A.C. Fonseca, M. Costa, I.F. Amaral, M.A. Barbosa, A.P. Águas, J.N. Barbosa, Macrophage polarization following chitosan implantation, Biomaterials 34 (2013) 9952–9959, doi:10.1016/j.biomaterials.2013.09.012.
[18] D. Yang, K.S. Jones, Effect of alginate on innate immune activation of macrophages, J. Biomed. Mater. Res. - Part A. 90 (2009) 411–418, doi:10.1002/jbm.a.32096.
[19] B.N. Brown, R. Londono, S. Tottey, L. Zhang, K.A. Kukla, M.T. Wolf, K.A. Daly, J.E. Reing, S.F. Badylak, Macrophage phenotype as a predictor of constructive remodeling following the implantation of biologically derived surgical mesh materials, Acta Biomater 8 (2012) 978–987, doi:10.1016/j.actbio.2011.11.031.
[20] A. Vishwakarma, N.S. Bhise, M.B. Evangelista, J. Rouwkema, M.R. Dokmeci, A.M. Ghaemmaghami, N.E. Vrana, A. Khademhosseini, Engineering Immunomodulatory Biomaterials To Tune the Inflammatory Response, Trends Biotechnol 34 (2016) 470–482, doi:10.1016/j.tibtech.2016.03.009.
[21] J.E. Rayahin, J.S. Buhrman, Y. Zhang, T.J. Koh, R.A. Gemeinhart, High and Low Molecular Weight Hyaluronic Acid Differentially Influence Macrophage Activation, ACS Biomater. Sci. Eng. 1 (2015) 481–493, doi:10.1021/acsbiomaterials.5b00181.
[22] V.K. Rangasami, S. Samanta, V.S. Parihar, K. Asawa, K. Zhu, O.P. Varghese, Y. Teramura, B. Nilsson, J. Hilborn, R.A. Harris, O.P. Oommen, Harnessing hyaluronic

acid-based nanoparticles for combination therapy: a novel approach for suppressing systemic inflammation and to promote antitumor macrophage polarization, Carbohydr. Polym. 254 (2021) 117291, doi:10.1016/j.carbpol.2020.117291.

[23] V.Y. Kosovrasti, L.V. Nechev, M.M. Amiji, Peritoneal Macrophage-Specific TNF-α Gene Silencing in LPS-Induced Acute Inflammation Model Using CD44 Targeting Hyaluronic Acid Nanoparticles, Mol. Pharm. 13 (2016) 3404–3416, doi:10.1021/acs.molpharmaceut.6b00398.

[24] T.J. Beldman, M.L. Senders, A. Alaarg, C. Pérez-Medina, J. Tang, Y. Zhao, F. Fay, J. Deichmöller, B. Born, E. Desclos, N.N. Van Der Wel, R.A. Hoebe, F. Kohen, E. Kartvelishvily, M. Neeman, T. Reiner, C. Calcagno, Z.A. Fayad, M.P.J. De Winther, E. Lutgens, W.J.M. Mulder, E. Kluza, Hyaluronan Nanoparticles Selectively Target Plaque-Associated Macrophages and Improve Plaque Stability in Atherosclerosis, ACS Nano 11 (2017) 5785–5799, doi:10.1021/acsnano.7b01385.

[25] O.P. Oommen, J. Garousi, M. Sloff, O.P. Varghese, Tailored doxorubicin-hyaluronan conjugate as a potent anticancer glyco-drug: an alternative to prodrug approach, Macromol. Biosci. 14 (2014) 327–333, doi:10.1002/mabi.201300383.

[26] O.P. Oommen, C. Duehrkop, B. Nilsson, J. Hilborn, O.P. Varghese, Multifunctional Hyaluronic Acid and Chondroitin Sulfate Nanoparticles: impact of Glycosaminoglycan Presentation on Receptor Mediated Cellular Uptake and Immune Activation, ACS Appl. Mater. Interfaces. 8 (2016) 20614–20622, doi:10.1021/acsami.6b06823.

[27] O.P. Oommen, S. Wang, M. Kisiel, M. Sloff, J. Hilborn, O.P. Varghese, Smart Design of Stable Extracellular Matrix Mimetic Hydrogel: synthesis, Characterization, and In Vitro and In Vivo Evaluation for Tissue Engineering, Adv. Funct. Mater. 23 (2013) 1273–1280, doi:10.1002/adfm.201201698.

[28] D. Bermejo-Velasco, S. Kadekar, M.V. Tavares Da Costa, O.P. Oommen, K. Gamstedt, J. Hilborn, O.P. Varghese, First Aldol Cross-Linked Hyaluronic Acid Hydrogel: fast and Hydrolytically Stable Hydrogel with Tissue Adhesive Properties, ACS Appl. Mater. Interfaces 11 (2019) 38232–38239, doi:10.1021/acsami.9b10239.

[29] M. Paidikondala, V.K. Rangasami, G.N. Nawale, T. Casalini, G. Perale, S. Kadekar, G. Mohanty, T. Salminen, O.P. Oommen, O.P. Varghese, An Unexpected Role of Hyaluronic Acid in Trafficking siRNA Across the Cellular Barrier: the First Biomimetic, Anionic, Non-Viral Transfection Method, Angew. Chemie Int. Ed. 58 (2019) 2815–2819, doi:10.1002/anie.201900099.

[30] H.J. Yan, T. Casalini, G. Hulsart-Billström, S. Wang, O.P. Oommen, M. Salvalaglio, S. Larsson, J. Hilborn, O.P. Varghese, Synthetic design of growth factor sequestering extracellular matrix mimetic hydrogel for promoting in vivo bone formation, Biomaterials 161 (2018) 190–202, doi:10.1016/j.biomaterials.2018.01.041.

[31] J.Y. Lai, L.J. Luo, Antioxidant gallic acid-functionalized biodegradable in situ gelling copolymers for cytoprotective antiglaucoma drug delivery systems, Biomacromolecules 16 (2015) 2950–2963, doi:10.1021/acs.biomac.5b00854.

[32] B. Badhani, N. Sharma, R. Kakkar, Gallic acid: a versatile antioxidant with promising therapeutic and industrial applications, RSC Adv 5 (2015) 27540–27557, doi:10.1039/c5ra01911g.

[33] M.F. Queiroz, D.A. Sabry, G.L. Sassaki, H.A.O. Rocha, L.S. Costa, Gallic acid-dextran conjugate: green synthesis of a novel antioxidant molecule, Antioxidants 8 (2019), doi:10.3390/antiox8100478.

[34] M. Shin, H. Lee, Gallol-Rich Hyaluronic Acid Hydrogels: shear-Thinning, Protein Accumulation against Concentration Gradients, and Degradation-Resistant Properties, Chem. Mater. 29 (2017) 8211–8220, doi:10.1021/acs.chemmater.7b02267.

[35] S. Samanta, V.K. Rangasami, N.A. Murugan, V.S. Parihar, O.P. Varghese, O.P. Oommen, An unexpected role of an extra phenolic hydroxyl on the chemical reactivity and bioactivity of catechol or gallol modified hyaluronic acid hydrogels, Polym. Chem. 12 (2021) 2987–2991, doi:10.1039/d1py00013f.

[36] M.H. Abnosi, S. Yari, The toxic effect of gallic acid on biochemical factors, viability and proliferation of rat bone marrow mesenchymal stem cells was compensated by boric acid, J. Trace Elem. Med. Biol. 48 (2018) 246–253, doi:10.1016/j.jtemb.2018.04.016.

[37] Y. Bi, J. Chen, F. Hu, J. Liu, M. Li, L. Zhao, M2 Macrophages as a Potential Target for Antiatherosclerosis Treatment, Neural Plast (2019) 2019, doi:10.1155/2019/6724903.

[38] Y. Yue, X. Yang, K. Feng, L. Wang, J. Hou, B. Mei, H. Qin, M. Liang, G. Chen, Z. Wu, M2b macrophages reduce early reperfusion injury after myocardial ischemia in mice: a predominant role of inhibiting apoptosis via A20, Int. J. Cardiol. 245 (2017) 228–235, doi:10.1016/j.ijcard.2017.07.085.

[39] J.C. Gensel, B. Zhang, Macrophage activation and its role in repair and pathology after spinal cord injury, Brain Res 1619 (2015) 1–11, doi:10.1016/j.brainres.2014.12.045.

[40] A.P. Hutchins, D. Diez, D. Miranda-Saavedra, The IL-10/STAT3-mediated anti-inflammatory response: recent developments and future challenges, Brief. Funct. Genomics. 12 (2013) 489–498, doi:10.1093/bfgp/elt028.

[41] K.N. Couper, D.G. Blount, E.M. Riley, IL-10: the Master Regulator of Immunity to Infection, J. Immunol. 180 (2008) 5771–5777, doi:10.4049/jimmunol.180.9.5771.

[42] J. Weischenfeldt, B. Porse, Bone Marrow-Derived Macrophages (BMM): isolation and Applications, Cold Spring Harb. Protoc. (2008) 2008pdb.prot5080, doi:10.1101/PDB.PROT5080.

[43] A. dos, Anjos Cassado, F4/80 as a major macrophage marker: the case of the peritoneum and spleen, in: Results Probl. Cell Differ., Springer Verlag, 2017, pp. 161–179, doi:10.1007/978-3-319-54090-0_7.

[44] C. Atri, F. Guerfali, D. Laouini, Role of Human Macrophage Polarization in Inflammation during Infectious Diseases, Int. J. Mol. Sci. 19 (2018) 1801, doi:10.3390/ijms19061801.

[45] M. Burgess, K. Wicks, M. Gardasevic, K.A. Mace, Cx3CR1 Expression Identifies Distinct Macrophage Populations That Contribute Differentially to Inflammation and Repair, ImmunoHorizons 3 (2019) 262–273, doi:10.4049/immunohorizons.1900038.

[46] C.M. Freria, J.C.E. Hall, P. Wei, Z. Guan, D.M. McTigue, P.G. Popovich, Deletion of the fractalkine receptor, CX3CR1, improves endogenous repair, axon sprouting, and synaptogenesis after spinal cord injury in mice, J. Neurosci. 37 (2017) 3568–3587, doi:10.1523/JNEUROSCI.2841-16.2017.

[47] C. O'Carroll, A. Fagan, F. Shanahan, R.J. Carmody, Identification of a Unique Hybrid Macrophage-Polarization State following Recovery from Lipopolysaccharide Tolerance, J. Immunol. 192 (2014) 427–436, doi:10.4049/JIMMUNOL.1301722.

[48] G. Liu, X. Xia, S. Gong, Y. Zhao, The macrophage heterogeneity: difference between mouse peritoneal exudate and splenic F4/80+ macrophages, J. Cell. Physiol. 209 (2006) 341–352, doi:10.1002/JCP.20732.

[49] D.L. Morris, K.E. Oatmen, T.A. Mergian, K.W. Cho, J.L. DelProposto, K. Singer, C. Evans-Molina, R.W. O'Rourke, C.N. Lumeng, CD40 promotes MHC class II expression on adipose tissue macrophages and regulates adipose tissue CD4 + T cells with obesity, J. Leukoc. Biol. 99 (2016) 1107–1119, doi:10.1189/jlb.3a0115-009r.

[50] E. Nova-Lamperti, G. Fanelli, P.D. Becker, P. Chana, R. Elgueta, P.C. Dodd, G.M. Lord, G. Lombardi, M.P. Hernandez-Fuentes, IL-10-produced by human transitional B-cells down-regulates CD86 expression on B-cells leading to inhibition of CD4+T-cell responses, Sci. Reports 6 (2016) 1–8 2016 61, doi:10.1038/srep20044.

[51] D.H. Madsen, D. Leonard, A. Masedunskas, A. Moyer, H.J. Jürgensen, D.E. Peters, P. Amornphimoltham, A. Selvaraj, S.S. Yamada, D.A. Brenner, S. Burgdorf, L.H. Engelholm, N. Behrendt, K. Holmbeck, R. Weigert, T.H. Bugge, M2-like macrophages are responsible for collagen degradation through a mannose receptor-mediated pathway, J. Cell Biol. 202 (2013) 951–966, doi:10.1083/jcb.201301081.

[52] D. Hachim, S.T. Lopresti, R.D. Rege, Y. Umeda, A. Iftikhar, A.L. Nolfi, C.D. Skillen, B.N. Brown, Distinct macrophage populations and phenotypes associated with IL-4 mediated immunomodulation at the host implant interface, Biomater. Sci. 8 (2020) 5751–5762, doi:10.1039/D0BM00568A.

[53] R.G. Rosique, M.J. Rosique, J.A. Farina Junior, Curbing inflammation in skin wound healing: a review, Int. J. Inflam. (2015) 2015, doi:10.1155/2015/316235.